Research Paper

Into the spongy-verse: structural differences between leaf and flower mesophyll

Running title: Structural mesophyll differences

Jeroen D.M. Schreel[1,2,*], Guillaume Théroux-Rancourt[3], Pamela K. Diggle[4], Craig Brodersen[5], Adam B. Roddy[1]

[1]Institute of Environment, Department of Biological Sciences, Florida International University, Miami, FL, USA, 33199

[2]Plant Sciences Unit, Flanders Research Institute for Agriculture, Fisheries and Food (ILVO), B-9090 Melle, Belgium

[3]Smart farming, Biopterre - Bioproducts development center, Sainte-Anne-de-la-Pocatière, Québec, Canada

[4]Department of Ecology and Evolutionary Biology U-3043, 75 N. Eagleville Rd, University of Connecticut, Storrs, CT, USA, 06269

[5]School of the Environment, Yale University, New Haven, CT, USA, 06520

[*]Corresponding author: jeroen.schreel@gmail.com

Structural mesophyll differences

Contact information: J.D.M.S.: jeroen.schreel@gmail.com
ORCID: 0000-0002-6152-1307
G.T.R.: guillaume.theroux-rancourt@biopterre.com
ORCID: 0000-0002-2591-0524
P.K.D.: pamela.diggle@uconn.edu
ORCID: 0000-0001-7391-0249
C.B.: craig.brodersen@yale.edu
ORCID: 0000-0002-0924-2570
A.B.R.: aroddy@fiu.edu
ORCID: 0000-0002-4423-8729

Number of tables: 2
Number of figures: 8
Black & White: Fig. 1-8

Word count:		
	Introduction:	1250
	Materials and Methods	1566
	Results and Discussion	1574
	Total	4390

Supplementary data: 2 tables, 7 figures

Highlights

While spongy mesophyll tissue occurs in both leaves and the flower perianth, this tissue is structurally different in the two organs.

Abstract

As the site of almost all terrestrial carbon fixation, the mesophyll tissue is critical to leaf function. However, mesophyll tissue is not restricted only to leaves but also occurs in the laminar, heterotrophic organs of the floral perianth, providing a powerful test of how metabolic differences are linked to differences in tissue structure. Here, we compared mesophyll tissues of leaves and flower perianths of six species using high-resolution X-ray computed microtomography (microCT) imaging. Consistent with previous studies, stomata were nearly absent from flowers, and flowers had a significantly lower vein density compared to leaves. However, mesophyll porosity was significantly higher in flowers than in leaves, and higher mesophyll porosity was associated with more aspherical mesophyll cells. Despite these differences in cell and tissue structure between leaf and flower mesophyll, modeled intercellular airspace conductance did not differ significantly between organs, regardless of differences in stomatal density between organs. These results suggest that in addition to differences between leaves and flowers in vein and stomatal densities, the mesophyll cells and tissues inside these organs also exhibit marked differences that may allow for flowers to be relatively cheaper in terms of biomass investment per unit of flower surface area.

Keywords

flower, flower anatomy, functional plant anatomy, intercellular airspace, leaf, leaf anatomy, microCT, spongy mesophyll, structure-function relations

Introduction

Photosynthesis and transpirational water loss are mechanistically linked through stomatal conductance, intercellular airspace conductance, and leaf vein density (Brodribb et al. 2007; de Boer et al. 2012). To facilitate CO_2 diffusion from the atmosphere into a leaf, the leaf needs to maintain a high surface conductance, which is accomplished by having high stomatal densities. Throughout the history of flowering plants, increasing leaf surface conductance occurred primarily through reductions in the size of stomatal pores and increases in their packing densities (Franks and Beerling 2009). To avoid desiccation, increases in leaf vein density have co-occurred with increasing stomatal conductance, balancing the increase in transpirational water loss with an increase in water supply (de Boer et al. 2012; Scoffoni et al. 2016; Brodribb et al. 2017).

The mesophyll, the tissue where chloroplasts fix CO_2, fills a substantial proportion of the leaf volume, sandwiched between the two epidermal layers, and is located between the veins. Unlike other tissues, the mesophyll is defined not only by its cellular features but also by the intercellular airspace that forms a network between the cells. Because CO_2 must diffuse through this intercellular airspace before entering the mesophyll cells, the conductance of the intercellular airspace is directly related to the organization of the mesophyll cells and tissue (Evans et al. 2009; Tomás et al. 2013; Earles et al. 2018; Théroux-Rancourt et al. 2021, 2023). In many leaves, mesophyll tissue is subdivided into adaxial palisade and abaxial spongy layers, which have distinct structures and functions. Palisade mesophyll tissue absorbs more light and fixes more carbon due to its adaxial position and densely packed, columnar-shaped cells (Ustin et al. 2001). The spongy mesophyll, by contrast, is typically more porous and lacks clear structural organization in some taxa, while it is highly ordered in others (Borsuk et al. 2022). What we know about mesophyll structure and organization is entirely dominated by the study of leaves; however, mesophyll tissue also occurs in non-photosynthetic, floral perianth organs. Understanding the structure and organization of mesophyll tissue in photosynthetic (i.e., leaves) and non-photosynthetic organs (e.g., petals) can illuminate how different functional demands can result in different structural organizations in homologous tissues.

The laminar, non-reproductive organs of flowers that comprise the floral perianth vary considerably among angiosperm lineages (Endress 2001). Floral perianths differentiated into distinct sepals and petals have evolved repeatedly among the

angiosperms, and petals are thought to have been derived from either stamen-like structures (andropetaloidy) or bract- or leaf-like structures (bracteopetaloidy) depending on their lineage (Eames 1961; Weberling 1989; Takhtajan 1991; Irish 2009). Despite starting development with similar structures (i.e., highly packed, confluent cells), foliar and floral mesophyll undergo different developmental trajectories that result in different mature structures, presumably because of different functional demands that have driven the evolution of these different developmental paths. While organs such as bracts, sepals, pedicels, ovaries, and fruits are capable of some photosynthesis (see Werk and Ehleringer (1983) and Galen *et al.* (1993)), most floral organs are thought to assimilate little to no CO_2. This lack of photosynthetic capacity has been predicted to have cascading consequences on the tissue structure of laminar, non-reproductive floral organs of the perianth, such as tepals and petals, potentially releasing them from selection for high rates of CO_2 diffusion (Roddy 2019).

First, efficient gas exchange is not a major selection pressure given that heterotrophic organs do not assimilate CO_2 (Lipayeva 1989; Roddy et al. 2016; Zhang et al. 2018), explaining why stomatal densities in leaves are 7 to 250 times higher than those in conspecific petals (Hew et al. 1980; Whiley et al. 1988; Blanke and Lovatt 1993; Liu et al. 2017; Zhang and Brodribb 2017; Roddy 2019). Strong phylogenetic structure has been observed in floral stomatal density, suggesting that there has been selection for reduced floral stomatal densities among more recently diverged angiosperm clades (Roddy et al. 2016; Ke et al. 2024).

Second, like in leaves (de Boer et al. 2012; Brodribb et al. 2017), stomatal density and vein density often covary in flowers (Roddy et al. 2016; Zhang et al. 2018; Ke et al. 2024). Without the need to transport high fluxes of water to support high rates of transpiration, flowers have lower abundances of veins traversing their petals compared to conspecific leaves (Roddy et al. 2013; Zhang et al. 2018; Roddy 2019; An et al. 2023).

Third, without the need to support high fluxes of CO_2 diffusion, the mesophyll of flowers may differ in its structural characteristics from that of leaves. Unlike leaves, which typically have two distinct layers of mesophyll — the palisade and the spongy layers — the floral mesophyll seems to be composed of only a porous spongy mesophyll layer (McCoy 1940; Satina and Blakeslee 1941; Kaplan 1968; Kay and Daoud 1981; Battey and Lyndon 1988).

The structure of floral mesophyll may influence how flowers perform different functions. While leaves must capture, scatter, and absorb light for photosynthesis, flowers often function as a visual attractor for pollinators. Like leaves (Bone et al. 1985; Vogelmann et al. 1996; Brodersen and Vogelmann 2007), many flowers have conically shaped epidermal cells that help to reflect light (Kay and Daoud 1981), a process that may be amplified by light scattering by the porous spongy mesophyll (Kay and Daoud 1981; Vogelman et al. 1996; Van Der Kooi et al. 2016; Van Der Kooi and Kelber 2022). In leaves, the porous structure of the spongy mesophyll is critical for CO_2 to diffuse from the stomatal pores and into the mesophyll cells and chloroplasts lining the mesophyll cell surfaces (Lundgren et al. 2019; Baillie and Fleming 2020; Théroux-Rancourt et al. 2021; Borsuk et al. 2022). In heterotrophic petals, however, maintaining CO_2 diffusion through the airspace and into the mesophyll cells has likely not been an important selection pressure in the evolution of mesophyll structure. Without selection for CO_2 diffusion, anatomical traits that influence diffusion may be more variable in flowers than in leaves, similar to the higher variability of hydraulic traits in flowers compared to leaves (Roddy et al. 2019; An et al. 2023). In addition to these optical and diffusional functions, the mesophyll may also perform a biomechanical role. Without carbon-rich veins to provide structural support, the mesophyll tissue of flowers, in combination with the epidermis, may act as a turgor-driven, hydrostatic skeleton (Roddy et al. 2019, 2023). In support of this hypothesis, the mesophyll tissue collapses and intercellular airspace porosity disappears when positive turgor pressure is lost in *Calycanthus occidentalis* tepals (Roddy et al. 2018). This line of evidence suggests that the different functions performed by floral and foliar mesophyll may result in divergent mesophyll organizations in the two organs.

In this paper, we compare the 3D structure of the mesophyll tissue in leaves and flowers using high-resolution X-ray micro-computed tomography (microCT) imaging. We chose six phylogenetically diverse species encompassing the breadth of floral physiological traits sampled to date (Roddy et al. 2016, 2023) (Table 1). We hypothesized that the absence of photosynthesis in flowers lowers their stomatal and vein densities. Because flowers are relatively short-lived, and have lower biomass costs per unit area (Roddy et al. 2023), we predicted that flower mesophyll may be thinner and more porous than leaf mesophyll. Because mesophyll porosity is accomplished by changes in cell shape (Zhang et al. 2021; Treado et al. 2022), we also predicted that flowers would have more aspherical

cells. However, because low stomatal densities (D_s) in flowers may effectively prevent diffusion even when the mesophyll is porous, we tested how D_s affects intercellular airspace conductance (g_{IAS}) by artificially varying D_s and calculating g_{IAS}.

Materials and Methods

Plant material

All plant material was collected from the living collections of the University of California Botanic Garden in Berkeley, CA, USA. We sampled leaves (n = 1) and flowers (n = 1) from six species that span known variation in floral hydraulic traits (Table 1). Previous sampling of floral anatomical and physiological traits suggests that there is relatively little intraspecific variation (Roddy et al. 2016; Zhang et al. 2018). Sampled shoots were taken from the top of the plant crown, though because all species were shrubs they experienced some shade. Shoots with recently opened flowers were excised in the early morning, and their cut ends immediately recut underwater and kept submerged in water to prevent tissue desiccation. Shoots were transported to the laboratory within 1 hour of collection. An approximately 5 x 10 mm piece of tissue was excised from midway down the length of petals and leaves and, for leaves, midway between the midrib and the leaf margin, avoiding major veins. This excised tissue was immediately enclosed in polyimide tape to prevent desiccation during microCT imaging and to aid in sample mounting. Samples were held in the X-ray beam by a cut pipette tip mounted in a drill chuck. The samples were positioned so that the X-ray beam passed through only polyimide tape and plant tissue.

X-ray micro-computed tomography (microCT) imaging

We used high resolution X-ray computed microtomography to image flower and leaf samples in three dimensions (Brodersen and Roddy 2016) at Beamline 8.3.2 of the Advanced Light Source of Lawrence Berkeley National Laboratory, Berkeley, CA, USA. Samples were scanned in continuous tomography mode at 24 keV as the samples rotated from 0° to 180°. The duration of each scan was between 5-7 minutes, and there was no visible damage to tissues after scanning. Images were captured by a camera (PCO EDGE; Cooke Corp., Romulus, MI, USA) with a 5x Mitutoyo long working distance lens. Scans resulted in 1,025 raw, two-dimensional tomographic projection images per sample, which

were then reconstructed using TomoPy (Gürsoy et al. 2014). Reconstructed scans were processed and mesophyll traits extracted using published methods (Théroux-Rancourt, Jenkins, et al. 2020) and briefly described below.

Leaf trait analysis of microCT images

Mesophyll thickness (L_{mes}; Table 2) was computed as the median height of all voxel columns throughout the sample. Tissue volumes were extracted as the sum of voxels per tissue type: veins (V_{vein}), mesophyll cells (V_{cell}), and intercellular airspace (V_{IAS}). Mesophyll volume (V_{mes}) was calculated as the sum of V_{cell} and V_{IAS}. Mesophyll porosity (θ_{IAS}) was calculated as V_{IAS}/V_{mes} (Théroux-Rancourt et al. 2023). Surface area of mesophyll cells exposed to the intercellular airspace (SA_{mes}) was computed by a marching cube algorithm (van der Walt et al. 2014) building surface meshes around the airspace using a step size of two (i.e., over every second voxel), which provides a surface area estimate for geometrical objects closer to their mathematical surface area than when using a step size of one (Théroux-Rancourt, Voggeneder, et al. 2020). Mesophyll surface area per projected leaf or petal surface area (S_m) was calculated as SA_{mes}/LA, where LA is the projected surface area of the sample stack (width × depth of the stack).

Stomatal density (D_s) was calculated as the number of stomata per LA. One species, *Bergenia crassifolia*, had amphistomatous leaves, while all other species had hypostomatous leaves. Flower tepals and petals had very few, if any, stomata (Table 1). Though they did not have stomata, *Romneya coulteri* petals had numerous cracks or pores in the petal epidermis (Fig. S2). While these pores were generally smaller than stomatal pores, they could nonetheless be pathways for gas diffusion, and so we treated them as stomata. Because the calculation of intercellular airspace conductance (g_{IAS}) from 3D mesophyll anatomy depends on the presence and spatial positioning of stomata (discussed below), we randomly added artificial stomata to floral tepal and petal epidermises. We performed a sensitivity analysis of the effects of stomatal density on g_{IAS} by using stomatal densities equivalent to 100%, 50%, and 25% of their conspecific leaf stomatal densities (Table S2). This allowed us to elucidate to what extent differences in diffusion capacity between leaves and flowers were due to differences in stomatal density versus mesophyll structure. For *Bergenia crassifolia*,

we added these stomata on both petal surfaces, reflecting the amphistomatous distribution on leaves.

We calculated a number of geometrical parameters that describe the organization of the porous mesophyll tissue (Earles et al. 2018). Lateral path lengthening (λ) is the increased path length for diffusion resulting from the discrete distribution of stomata and is calculated as L_{Euc}/L_{epi}, where L_{Euc} is the Euclidean path length from a stoma to a point along the mesophyll surface and L_{epi} is the epidermal path length (Earles et al. 2018; Théroux-Rancourt et al. 2023). In other words, L_{Euc} is the shortest unobstructed distance from a stoma to a point along the mesophyll surface, while L_{epi} is the distance from the abaxial epidermis for hypostomatous leaves, or the shortest distance from either the ad- or abaxial epidermis for amphistomatous leaves, to a point along the mesophyll surface. The tortuosity factor (τ) is the square of the ratio of the path length travelled by diffusion to the Euclidean path length, calculated as $(L_{geo}/L_{Euc})^2$, where L_{geo} is the geodesic path length or the actual path length travelled by a diffusing CO_2 molecule from the closest stoma to a point along the mesophyll surface (Earles et al. 2018; Théroux-Rancourt et al. 2023). Both the code used and a detailed description of the steps taken to measure these parameters are available at https://github.com/gtrancourt/leaf-traits-microct/tree/dev.

By combining these structural traits, we calculated the conductance of the intercellular airspace (g_{IAS}) as (Earles et al. 2018):

$$g_{IAS} = \frac{\theta_{IAS} D_m}{e L_{mes} \tau \lambda} \quad \text{Eq. 1}$$

where D_m represents the diffusion coefficient of CO_2 in air (16 $mm^2\ s^{-1}$) and eL_{mes} is the effective mesophyll thickness, considered to be 0.5 L_{mes} for hypostomataous leaves and 0.25 L_{mes} for amphistomatous leaves.

Vein density, or vein length per projected area (VLA), was calculated as the total length of veins divided by LA. We measured vein diameter manually by imposing three transects on a paradermal cross-section positioned to pass through the middle of the veins : two intersecting diagonal transects and one transect parallel to the edge of the paradermal cross section, separating the top quarter from the second quarter of the image. This pattern prevented the same point from being intersected by all three transects and also incorporated variation in measured diameter due to vein orientation. Though this approach results in an overestimation in vein diameter because the shortest vein diameter is that

perpendicular to the tangent of the vein at any point, this approach is similar to traditional methods for measuring vein diameter that rely on two-dimensional leaf cross-sections that cut veins obliquely.

Cell segmentation for quantifying cell shape

While previous segmentations of individual mesophyll cells from microCT image stacks relied on only one cell per scan (Théroux-Rancourt, Voggeneder, et al. 2020; Harwood et al. 2021), we manually segmented three cells (pseudoreplicates) of each mesophyll tissue type (spongy and/or palisade parenchyma) per scan to capture variation in cell shape. First, edges of the target cell in contact with surrounding cells were identified because cell walls are brighter in microCT images than cell interiors and because sharp changes in cell surface curvature occur at cell-cell boundaries. These cell-cell boundaries were manually delineated using a graphic tablet (Wacom Cintiq 16, Wacom Co, Saitama, Japan) in Fiji (Schindelin et al. 2021), making sure the cell wall of the target cell was inside the selected area and not covered by the line drawn. To completely detach the cell of interest from the surrounding tissue, multiple iterations of rotating and reslicing the stack were followed by identifying and drawing the contact edges. Second, the stack was thresholded using the built-in automated threshold function in Fiji. Subsequently, the cell of interest was manually flood-filled with a contrasting grey value. The colored stack was thresholded again using the built-in threshold function in Fiji, using a selected greyscale range that included only the colored cell. The segmented cell was smoothed by a median filter with a pixel radius of two and resliced three times to have equal smoothing in all directions (x, y, and z planes). Lastly, the surface area (A) and volume (V) of the cell was measured using the Particle Analyser function of the BoneJ plugin (Doube et al. 2010) for Fiji. A visualization of this workflow can be found in the supplement (Fig. S1).

Based on the surface area and volume of a cell, the cell's deviation from a perfect sphere, i.e., asphericity ($\mathcal{A}$), was calculated as:

$$\mathcal{A} = \frac{A^{\frac{3}{2}}}{6\,V\,\pi^{\frac{1}{2}}} \qquad \text{Eq. 2}$$

where $\mathcal{A}$ = 1 for a perfect sphere and increases with increasing asphericity (Treado et al. 2022).

Statistical analysis

Most variables, except VLA and SA_{mes}/V_{IAS}, exhibited more variance among flowers than among leaves. To take this difference in variance into account, we used paired t-tests with unequal variance (paired Welch's t-test) to compare traits between organs (i.e., leaves and flowers). To compare multiple datasets (e.g., flowers, leaf spongy mesophyll, leaf palisade mesophyll and all leaf mesophyll) a pairwise paired t-test with unequal variance was performed. We incorporated phylogenetic analyses where appropriate by constructing a dated supertree using V.Phylomaker2 (Jin and Qian 2022). Phylogenetic paired t-tests were used to compare flower and leaf traits (phyl.pairedttest() in R package *phytools* (Revell 2024)).All statistical tests were performed in R (R Core Team 2020).

Results and Discussion

Our comparison of leaf and flower 3D mesophyll structure highlights the diversity of mesophyll structures. Consistent with analyses of physiological traits (Roddy et al. 2019; An et al. 2023), our results show that for almost every mesophyll trait measured, flowers exhibited higher interspecific variability than leaves. While mesophyll porosity is important to facilitate CO_2 diffusion in leaves, high mesophyll porosity also potentially reduces the metabolic costs of tissue construction and maintenance, which may be critical in short-lived, heterotrophic organs like flower tepals and petals.

Stomata were almost completely absent on flowers, resulting in a significantly lower stomatal density for flowers compared to leaves ($t = 5.01$, $df = 5$, $p < 0.05$). Leaf stomatal density ranged from 43 to 553 mm^{-2}, depending on species (Table 1). By contrast, we found stomata on flowers of only two species, *Illicium floridanum* and *Rhododendron mucronatum*, though petals of *Romneya coulteri* had numerous epidermal pores that could allow for gas exchange between the petal interior and the atmosphere (Fig. S2; Table 1). Fewer stomata on flowers should decrease transpirational water loss, allowing for lower VLA in flowers. Consistent with previous findings (Feild et al. 2009; Roddy et al. 2013; Zhang et al. 2018; An et al. 2023), VLA was significantly lower in flowers compared to leaves ($t = -4.91$, $df = 5$, $p < 0.05$; Fig. 1, Table S1). As a result, flowers must hydrate a larger mesophyll volume per unit of vein volume (V_{mes}/V_{vein}; $t = 2.01$, $df = 5$, $p < 0.10$; Fig. 1). Despite this consistent difference in VLA, vein diameter was not significantly different between organ types ($p = 0.66$), and

flowers exhibited much greater variation in vein diameter than did leaves (Fig. 1). This larger variance is a result of two contrasting groups of species: those in which flowers have narrower veins than their conspecific leaves (*Luculia gratissima*, *Rhododendron mucronatum*, and *Romneya coulteri*) and those in which flowers have wider veins than their conspecific leaves (*Bergenia crassifolia*, *Camellia yunnanensis*, and *Illicium floridanum*) (Fig. S3). While narrower petal/tepal veins could be due to lower transpirational demand, thicker floral veins could compensate for lower VLA to achieve similar water supply. However, without more information about conduit number per vein and conduit diameter, it is difficult to draw clear conclusions. Furthermore, only the difference in VLA between organs remained significant after accounting for shared evolutionary history (Table S1), though this is likely due to the small number of species in our study.

As flowers function mainly as pollinator attractors, the structure and organization of the mesophyll were predicted to differ between leaves and flowers. Attracting pollinators requires large, showy floral displays that reflect light externally, e.g., through conical epidermal cells and reflective mesophyll surfaces (Kay and Daoud 1981; Van Der Kooi et al. 2016). Contrary to flowers, leaves need to capture and scatter light internally to be absorbed by mesophyll tissue for photosynthesis, which requires large mesophyll tissue volumes to maximize light absorption. Due to these differences in function and associated mesophyll thickness and volumes, flower mesophyll thickness (L_{mes}) and porosity (θ_{IAS}) were expected to be lower and higher compared to their conspecific leaves, respectively.

Contrary to our initial hypothesis, the overall difference in L_{mes} between flowers and leaves was insignificant, with only *Bergenia crassifolia* and *Romneya coulteri* having a lower L_{mes} in flowers than leaves (Figs. 2 and 3). All else being equal, thinner mesophyll would reduce floral carbon construction costs per unit area (Roddy et al. 2023). That most species exhibited thicker L_{mes} in flowers than leaves is surprising, but may due to biomechanics; tissue thickness increases stiffness independently of the material properties.

Thicker mesophyll in flowers may compensate for the biomechanical effects of higher porosity in flowers. Because selection may have favored reduced biomass costs in flowers compared to leaves, one of the primary ways of accomplishing this would have been through a higher mesophyll porosity (θ_{IAS}) (Roddy et al. 2023). Even though we sampled only six species, flowers exhibited almost the full range (0-1) of mesophyll porosities that are physically possible, ranging from 0.11 in *I. floridanum* to 0.76 in *L. gratissima*. θ_{IAS} was

marginally higher in flowers compared to leaves ($t = 2.01$, $df = 5$, $p < 0.10$) and consistently higher in flowers for every species except *I. floridanum* (Fig. 2), suggesting that while mesophyll volume per unit projected surface area (V_{mes}/LA) was not significantly different between flowers and leaves, floral mesophyll is generally more porous. This higher porosity would contribute to lower biomass costs per unit area for flowers (Roddy et al. 2023). While higher porosity could reduce organ stiffness, thicker L_{mes} in flowers could compensate for higher porosity. The lower θ_{IAS} for the entire leaf mesophyll is due primarily to the densely packed palisade mesophyll, which is absent in flowers (Fig. 3). However, with the exception of *I. floridanum*, the spongy mesophyll in flowers is more porous than even the leaf spongy mesophyll (Fig. 4). The wide diversity in mesophyll thickness and porosity of flowers observed in just these six species could be due to variation in other ecological factors.

Given that the proto-mesophyll tissue in leaf and flower primordia begins development as highly packed (i.e. almost no porosity) but then matures into a wide range of mesophyll porosities (Fig. 2 and 3), we asked whether this variation in tissue porosity is driven by similarly wide variation in cell shape. Recent modeling and visualization of *Arabidopsis* mesophyll development has shown that the development of spongy mesophyll porosity is driven by changes in cell shape towards increasingly lobed, more aspherical shapes (Maksymowych 1973; Zhang et al. 2021; Treado et al. 2022). Additionally, among widely divergent vascular plant lineages, leaf spongy mesophyll in many species exhibits a highly conserved structural organization composed of lobed cells that form a stable network (Borsuk et al. 2022).

Among the species sampled here, flowers tended to have both more porous mesophyll tissue (Fig. 3 and4) and mesophyll cells that were more aspherical than leaves (Fig 3 and 5). Across the spongy mesophyll of both leaves and flowers, cell shape asphericity ($\mathcal{A}$) and tissue porosity (θ_{IAS}) were strongly coordinated ($p < 0.05$; Fig. 6), suggesting that cell shape–and not only the organization of cells in 3D–is a critical determinant of mesophyll tissue-level porosity. The higher $\mathcal{A}$ and θ_{IAS} in flowers may, therefore, be central traits enabling petals to be biomechanically robust yet have a low dry mass per area. Because mesophyll cells must remain in contact with each other, increasing tissue-level porosity seems to require more aspherical cells (Fig. 6).

Variation in stomatal density (D_s) and θ_{IAS} affected both the Euclidean path length (L_{Euc}) and the geodesic path length (L_{geo}) from a stoma to a point along the mesophyll surface. Low D_s led to increases in L_{Euc} and lateral path lengthening (λ; Fig. 7), and a decrease in θ_{IAS} resulted in a low L_{geo} and tortuosity factor (τ) (Earles et al. 2018). Because current methods for estimating conductance through the intercellular airspace (g_{IAS}) require tracing the paths from stomata to the mesophyll cell surfaces, estimating g_{IAS} requires knowing where stomata are. Thus, having few or no stomata would preclude calculating g_{IAS}. Yet, intercellular airspace conductance can be calculated even if there is no concentration gradient to drive the flux. To overcome this methodological limitation for flowers without stomata, we artificially added stomata in varying densities to petals and tepals and calculated the resulting g_{IAS}. Decreasing Ds tended to cause λ to increase, with major changes occurring between 50% and 25% of leaf Ds, though differences between leaves and flowers with equal D_s were not significantly different (Fig. 7). Thus, g_{IAS} may be relatively constant across a wide range of Ds under the θ_{IAS} observed here, indicating that the stomatal resistance is much higher than other gas-phase components of the diffusional pathway. τ was expected to be influenced to some extent by Ds and θ_{IAS}; however, decreasing Ds (Fig. S4) or varying θ_{IAS} (Fig. S5) appeared to have little effect on τ. The effects of D_s on τ at low porosity were likely due to the stochastic positioning of stomata that occurs at low D_s (Fig. S5). Based on the limited effect of Ds on λ and τ, it is not surprising that the effect of Ds on g_{IAS} was also limited and not significantly different between leaf and flower spongy mesophyll (Fig. 8), nor when examining the entire leaf mesophyll (spongy and palisade together) (Fig. S6).

Conclusions

Using a novel dataset of 3D mesophyll structure for conspecific leaves and flowers, we characterized the differences between organs in mesophyll structure and function. The lower stomatal and vein densities observed in flowers compared to leaves were associated with differences in mesophyll structure. Aside from a reduction in carbon-dense veins among flowers, mesophyll porosity was significantly higher in flowers than in leaves, explaining at least partially why flowers have lower biomass costs per unit of area. Despite these large structural differences in the mesophyll of flowers and leaves, intercellular airspace conductance did not differ significantly between leaves and flowers when flowers

were artificially given stomatal densities on par with leaves. This result reiterates the importance of low stomatal densities on flowers in protecting their porous mesophyll from the desiccating atmosphere. Importantly, across both leaves and flowers, increasing spongy mesophyll porosity was associated with more aspherical mesophyll cells. Together, these results highlight how different functional demands and developmental trajectories can give rise to a diversity of forms.

Acknowledgements

The authors thank D.Y. Parkinson for help at the microCT beamline, and H. Forbes for facilitating access to plants at the U.C. Botanical Garden.

Funding

This work was supported by a fellowship from the Yale Institute for Biospheric Studies to A.B.R. and by US NSF grant CMMI-2029756 to A.B.R. and C.R.B. The Advanced Light Source is supported by the Director, Office of Science, Office of Basic Energy Sciences, of the US Department of Energy under contract no. DE-AC02-05CH11231.

Competing interests

The authors declare no conflict of interest.

Author contributions

The project was conceptualized by A.B.R., P.K.D., and C.R.B. Original scans were collected by A.B.R., G.T.-R. C.R.B. Data were processed and analyzed by J.D.M.S., G.T.R., and A.B.R. Conceptualization and writing of the original draft was done by J.D.M.S. Writing, reviewing and editing was done by all co-authors. The project was supervised by A.B.R.

Data availability

The primary data supporting this study were not made publicly available at the time of publication, but can be made available upon request.

References

An Y-D, Roddy AB, Zhang T-Z, Jiang G-F. 2023. Hydraulic differences between flowers and leaves are driven primarily by pressure-volume traits and water loss. Frontiers in Plant Science 14:Article: 1130724.

Baillie AL, Fleming AJ. 2020. The developmental relationship between stomata and mesophyll airspace. New Phytologist 225:1120–26.

Battey NH, Lyndon RF. 1988. Determination and differentiation of leaf and petal primordia in *Impatiens balsamina*. Annals of Botany 61:9–16.

Blanke MM, Lovatt CJ. 1993. Anatomy and transpiration of the avocado inflorescence. Annals of Botany 71:543–47.

Bone RA, Lee DW, Norman JM. 1985. Epidermal cells functioning as lenses in leaves of tropical rain-forest shade plants. Applied Optics 24:1408–12.

Borsuk AM, Roddy AB, Théroux-Rancourt G, Brodersen CR. 2022. Structural organization of the spongy mesophyll. New Phytologist 234:946–60.

Brodersen CR, Roddy AB. 2016. New frontiers in the three-dimensional visualization of plant structure and function. American Journal of Botany 103:184–88.

Brodersen CR, Vogelmann TC. 2007. Do epidermal lens cells facilitate the absorptance of diffuse light? American Journal of Botany 94:1061–66.

Brodribb TJ, Feild TS, Jordan GJ. 2007. Leaf maximum photosynthetic rate and venation are linked by hydraulics. Plant Physiology 144:1890–98.

Brodribb TJ, McAdam SAM, Murphy MRC. 2017. Xylem and stomata, coordinated through time and space. Plant, Cell & Environment 40:872–80.

de Boer HJ, Eppinga MB, Wassen MJ, Dekker SC. 2012. A critical transition in leaf evolution facilitated the Cretaceous angiosperm revolution. Nature Communications 3:Article: 1221.

Doube M, Klosowski MM, Arganda-Carreras I, Cordelières FP, Dougherty RP, Jackson JS, Schmid B, Hutchinson JR, Shefelbine SJ. 2010. BoneJ: Free and extensible bone image analysis in ImageJ. Bone 47:1076–79.

Eames AJ. 1961. Morphology of the Angiosperms New York: McGraw-Hill.

Earles JM, Théroux-Rancourt G, Roddy AB, Gilbert ME, McElrone AJ, Brodersen CR. 2018. Beyond porosity: 3D leaf intercellular airspace traits that impact mesophyll conductance. Plant Physiology 178:148–62.

Endress PK. 2001. Origins of flower morphology. Journal of Experimental Zoology 291:105–15.

Evans JR, Kaldenhoff R, Genty B, Terashima I. 2009. Resistances along the CO_2 diffusion pathway inside leaves. Journal of Experimental Botany 60:2235–48.

Feild TS, Chatelet DS, Brodribb TJ. 2009. Giant flowers of Southern Magnolia are hydrated by the xylem. Plant Physiology 150:1587–97.

Franks PJ, Beerling DJ. 2009. Maximum leaf conductance driven by CO_2 effects on stomatal size and density over geologic time. Proceedings of the National Academy of Sciences 106:10343–47.

Galen C, Dawson TE, Stanton ML. 1993. Carpels as leaves: meeting the carbon cost of reproduction in an alpine buttercup. Oecologia 95:187–93.

Gürsoy D, De Carlo F, Xiao X, Jacobsen C. 2014. TomoPy: a framework for the analysis of synchrotron tomographic data. Journal of Synchrotron Radiation 21:1188–93.

Harwood R, Théroux-Rancourt G, Barbour MM. 2021. Understanding airspace in leaves: 3D anatomy and directional tortuosity. Plant, Cell & Environment 44:2455–65.

Hew CS, Lee GL, Wong SC. 1980. Occurrence of non-functional stomata in the flowers of tropical orchids. Annals of Botany 46:195–201.
Irish VF. 2009. Evolution of petal identity. Journal of Experimental Botany 60:2517–27.
Jin Y, Qian H. 2022. V.PhyloMaker2: An updated and enlarged R package that can generate very large phylogenies for vascular plants. Plant Diversity 44:335–39.
Kaplan DR. 1968. Structure and development of the perianth in *Dowingia bacigalupii*. American Journal of Botany 55:406–20.
Kay QON, Daoud HS. 1981. Pigment distribution, light reflection and cell structure in petals. Botanical Journal of the Linnean Society 83:57–84.
Ke Y, Zhang Y □B., Zhang F □P., Yang D, Wang Q, Peng X □R., Huang X □Y., Sher J, Zhang J □L. 2024. Monocots and eudicots have more conservative flower water use strategies than basal angiosperms. Plant Biol J 26:621–32.
Lipayeva LI. 1989. On the anatomy of petals in angiosperms. Botanicheskii Zhurnal 74:9–18.
Liu H, Xu QY, Lundgren MR, Ye Q. 2017. Different water relations between flowering and leaf periods: a case study in flower-before-leaf-emergence *Magnolia* species. Functional Plant Biology 44:1098–1110.
Lundgren MR, Mathers A, Baillie AL, Dunn J, Wilson MJ, Hunt L, Pajor R, Fradera-Soler M, Rolfe S, Osborne CP, Sturrock CJ, Gray JE, Mooney SJ, Fleming AJ. 2019. Mesophyll porosity is modulated by the presence of functional stomata. Nature Communictions 10:Article: 2825.
Maksymowych R. 1973. Analysis of leaf development.
McCoy RW. 1940. Floral organogenesis in *Frasera carolinensis*. American Journal of Botany 27:600–609.
R Core Team. 2020. R: A language and environment for statistical computing. .
Revell LJ. 2024. phytools 2.0: an updated R ecosystem for phylogenetic comparative methods (and other things). PeerJ 12:Article: e16505.
Roddy AB. 2019. Energy Balance Implications of Floral Traits Involved in Pollinator Attraction and Water Balance. International Journal of Plant Sciences 180:944–53.
Roddy AB, Brodersen CR, Dawson TE. 2016. Hydraulic conductance and the maintenance of water balance in flowers. Plant, Cell & Environment 39:2123–32.
Roddy AB, Guilliams CM, Fine PVA, Mambelli S, Dawson TE, Simonin KA. 2023. Flowers are leakier than leaves but cheaper to build. New Phytologist 239:2076–82.
Roddy AB, Guilliams CM, Lilittham T, Farmer J, Wormser V, Pham T, Fine PVA, Feild TS, Dawson TE. 2013. Uncorrelated evolution of leaf and petal venation patterns across the angiosperm phylogeny. Journal of Experimental Botany 64:4081–88.
Roddy AB, Jiang GF, Cao K-F, Simonin KA, Brodersen CR. 2019. Hydraulic traits are more diverse in flowers than in leaves. New Phytologist 223:193–203.
Roddy AB, Simonin KA, McCulloh KA, Brodersen CR, Dawson TE. 2018. Water relations of Calycanthus flowers: Hydraulic conductance, capacitance, and embolism resistance. Plant, Cell & Environment 41:2250–62.
Satina S, Blakeslee AF. 1941. Periclinal chimeras in *Datura stramonium* in relation to development of leaf and flower. American Journal of Botany 28:862–71.
Schindelin J, Arganda-Carreras I, Frise E, Kaynig V, Longair M, Pietzsch T, Preibisch S, Rueden C, Saafeld S, Schmid B, Tinevez J-Y, White DJ, Hartenstein V, Eliceiri K, Tomancak P, Cardona A. 2021. Fiji: An open-source platform for biological-image analysis. Nature Methods 9:676–82.

Scoffoni C, Chatelet DS, Pasquet-kok J, Rawls M, Donoghue MJ, Edwards EJ, Sack L. 2016. Hydraulic basis for the evolution of photosynthetic productivity. Nature Plants 2:Article: 16072.

Takhtajan A. 1991. Evolutionary trends in flowering plants New York: Columbia University Press.

Théroux-Rancourt G, Herrera JC, Voggeneder K, De Berardinis F, Luijken N, Nocker L, Savi T, Scheffknecht S, Schneck M, Tholen D. 2023. Analyzing anatomy over three dimensions unpacks the differences in mesophyll diffusive area between sun and shade *Vitis vinifera* leaves. AoB PLANTS Article: plad001.

Théroux-Rancourt G, Jenkins MR, Brodersen CR, McElrone AJ, Forrestel EJ, Earles JM. 2020. Digitally deconstructing leaves in 3D using X-ray microcomputed tomography and machine learning. Applications in Plant Sciences 8:Article: e11380.

Théroux-Rancourt G, Roddy AB, Earles JM, Gilbert ME, Zwieniecki MA, Boyce CK, Tholen D, McElrone AJ, Simonin KA, Brodersen CR. 2021. Maximum CO_2 diffusion inside leaves is limited by the scaling of cell size and genome size. Proceedings of the Royal Society B 288:Article: 20203145.

Théroux-Rancourt G, Voggeneder K, Tholen D. 2020. Shape matters: the pitfalls of analyzing mesophyll anatomy. New Phytologist 225:2239–42.

Tomás M, Flexas J, Copolovici L, Galmés J, Hallik L, Medrano H, Ribas-Carbó M, Tosens T, Vislap V, Niinemets Ü. 2013. Importance of leaf anatomy in determining mesophyll diffusion conductance to CO_2 across species: quantitative limitations and scaling up by models. Journal of Experimental Botany 64:2269–81.

Treado JD, Roddy AB, Théroux-Rancourt G, Zhang L, Ambrose C, Brodersen CR, Shattuck MD, O'Hern CS. 2022. Localized growth and remodelling drives spongy mesophyll morphogenesis. Journal of the Royal Society Interface 19:Article: 20220602.

Ustin SL, Jacquemoud S, Govaerts Y. 2001. Simulation of photon transport in a three-dimensional leaf: implications for photosynthesis. Plant, Cell & Environment 24:1095–1103.

Van Der Kooi CJ, Elzenga JTM, Staal M, Stavenga DG. 2016. How to colour a flower: on the optical principles of flower coloration. Proc R Soc B 283:20160429.

Van Der Kooi CJ, Kelber A. 2022. Achromatic cues are important for flower visibility to hawkmoths and other insects. Front Ecol Evol 10:Article: 819436.

van der Walt S, Schönberger JL, Nunez-Iglesias J, Boulogne F, Warner JD, Yager N, Gouillart E, Yu T, the scikit-image contributors. 2014. scikit-imagej: Image processing in Python. PeerJ 2:Article: e453.

Vogelman TC, Nishio JN, Smith WK. 1996. Leaves and light capture: light propagation and gradients of carbon fixation within leaves. Trends in Plant Science 1:65–70.

Vogelmann TC, Bornman JF, Yates DJ. 1996. Focusing of light by leaf epidermal cells. Physiologia Plantarum 98:43–56.

Weberling F. 1989. Morphology of flowers and inflorescences Cambridge: Cambridge University Press.

Werk KS, Ehleringer JR. 1983. Photosynthesis by flowers in *Encelia farinosa* and *Encelia californica* (Asteraceae). Oecologia 57:311–15.

Whiley AW, Chapman KR, Saranah JB. 1988. Water loss by floral structures of avocado (Persea americana cv. Fuerte) during flowering. Australian Journal of Agricultural Research 39:457–67.

Zhang F-P, Brodribb TJ. 2017. Are flowers vulnerable to xylem cavitation during drought? Proceedings of the Royal Society B: Biological Sciences 284:Article: 20162642.

Zhang F-P, Carins Murphy MR, Cardoso AA, Jordan GJ, Brodribb TJ. 2018. Similar geometric rules govern the distribution of veins and stomata in petals, sepals and leaves. New Phytologist 219:1224–34.

Zhang L, McEvoy D, Le Y, Ambrose C. 2021. Live imaging of microtubule organization, cell expansion, and intercellular space formation in *Arabidopsis* leaf spongy mesophyll cells. The Plant Cell 33:623–41.

Tables

Table 1. Measured stomatal densities (stomata mm^{-2}) on the adaxial (AD) and abaxial (AB) surface (n = 1).

	Surface	Leaf	Flower
Bergenia crassifolia	AD	28	0
	AB	105	0
Camellia yunnanensis	AD	0	0
	AB	178	0
Illicium floridanum	AD	0	0
	AB	43	1
Luculia gratissima	AD	0	0
	AB	239	0
Rhododendron mucronatum	AD	0	0
	AB	239	5
Romneya coulteri	AD	0	0
	AB	553	260*

*Not real stomata, but pores that could be used for gas exchange

Table 2. Symbols and abbreviations with their units and description

Symbol	Unit	Description
$\mathcal{A}$	-	Asphericity
A	mm^2	Cell surface area
D_m	$mm^2\ s^{-1}$	Diffusion coefficient
D_s	stomata mm^{-2}	Stomatal density
g_{IAS}	$mm\ s^{-1}$	Intercellular airspace conductance
LA	mm^2	Projected surface area
L_{Euc}	mm	Euclidean path length
L_{epi}	mm	Epidermal path length
L_{geo}	mm	Geodesic path length or the actual path length
L_{mes}	mm	Mesophyll thickness
S_m	mm^2	Mesophyll surface area per projected leaf or petal surface area
SA_{mes}	mm^2	Surface area of mesophyll cells exposed to the intercellular airspace
V	mm^3	Cell volume
V_{cell}	mm^3	Volume of mesophyll cells
V_{IAS}	mm^3	Volume of mesophyll intercellular airspace
VLA	$mm\ mm^{-2}$	Vein density, or vein length per area
V_{mes}	mm^3	Volume of mesophyll
V_{vein}	mm^3	Vein volume
θ_{IAS}	$mm^3\ mm^{-3}$	Mesophyll porosity
λ	$mm\ mm^{-1}$	Lateral path lengthening
τ	$mm^2\ mm^{-2}$	Tortuosity factor

Figure legends

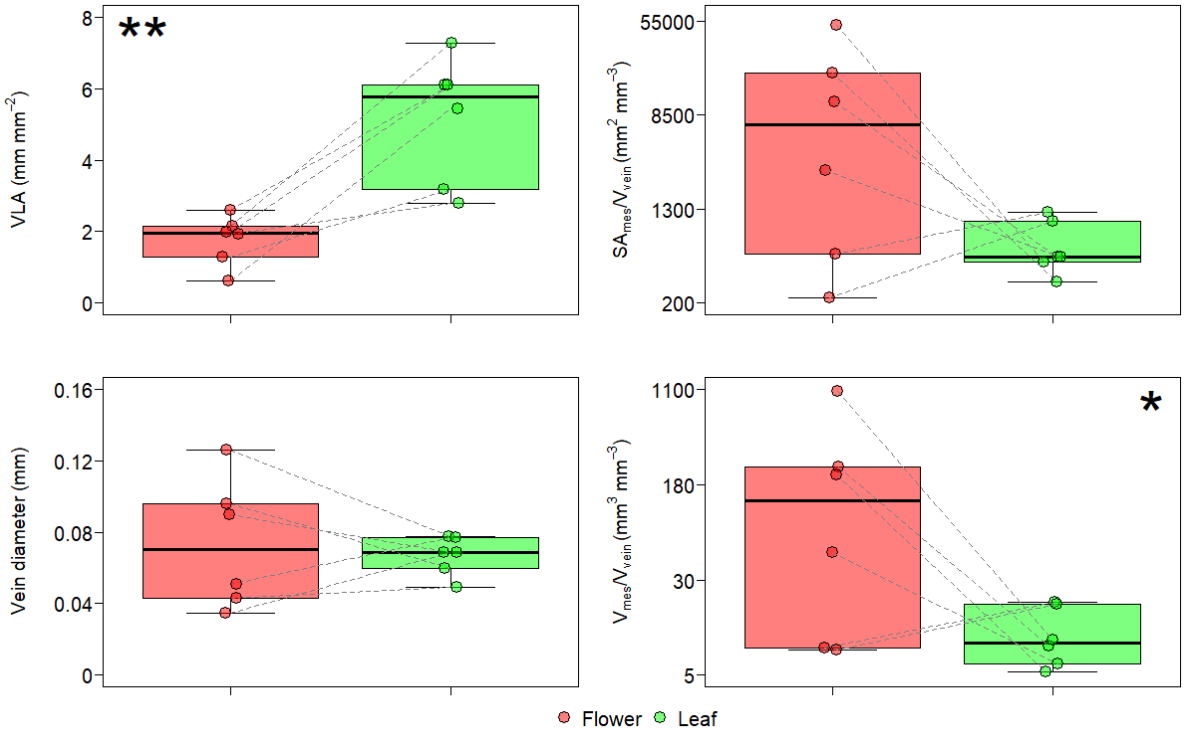

Fig. 1 Anatomical traits related to veins for the six species studied. For flowers (red) and leaves (green), vein density (VLA; mm mm^{-2}), mesophyll surface area exposed to the IAS per unit of vein volume (SA_{mes}/V_{vein}; mm^2 mm^{-3}), vein diameter (mm) and mesophyll volume per unit of vein volume (V_{mes}/V_{vein}; mm^3 mm^{-3}) are shown. * and ** displayed in plots indicate significant differences with $p < 0.10$ and $p < <0.05$, respectively.

Structural mesophyll differences

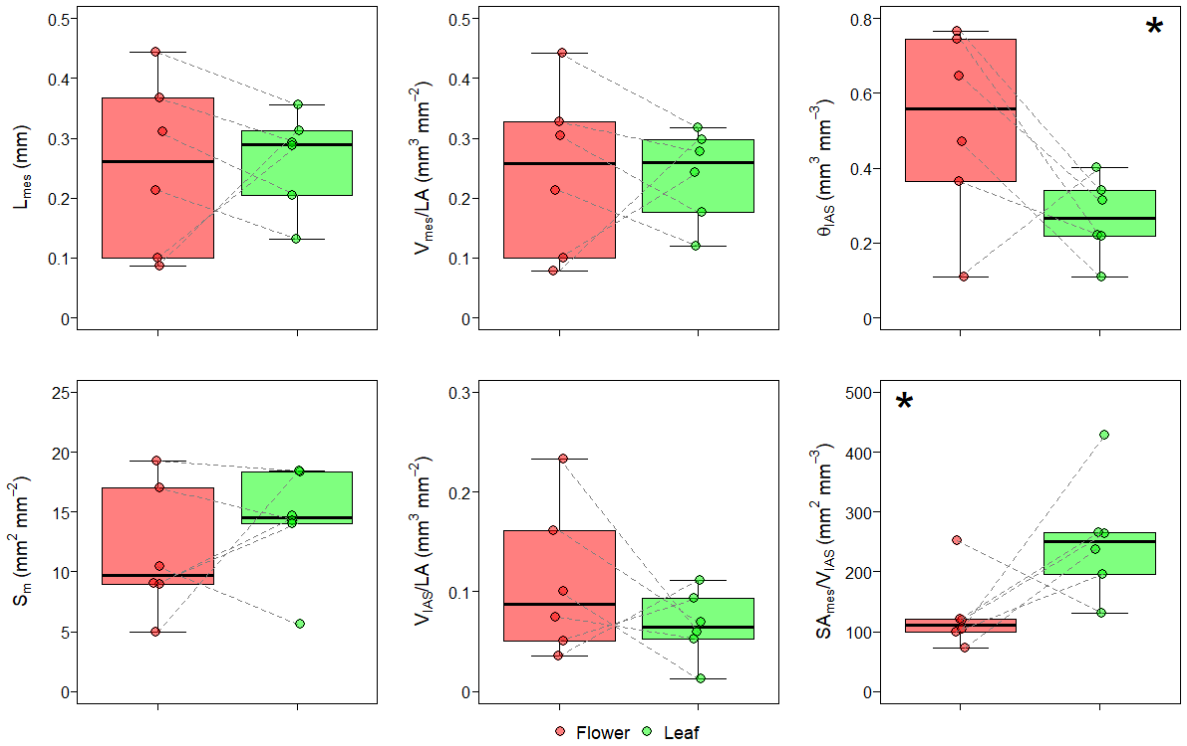

Fig. 2 Anatomical traits related to mesophyll tissue for the six species studied. For flowers (red) and leaves (green), mesophyll thickness (L_{mes}; mm), mesophyll volume per unit of leaf area (V_{mes}/LA; mm^3 mm^{-2}), mesophyll porosity (θ_{IAS}; mm^3 mm^{-3}), mesophyll surface area per projected area (S_m; mm^2 mm^{-2}), intercellular airspace volume per unit of leaf area (V_{IAS}/LA; mm^3 mm^{-2}) and mesophyll surface area exposed to the IAS per unit of intercellular airspace volume (SA_{mes}/V_{IAS}; mm^2 mm^{-3}) are shown. * displayed in plots indicate significant differences with $p < 0.10$.

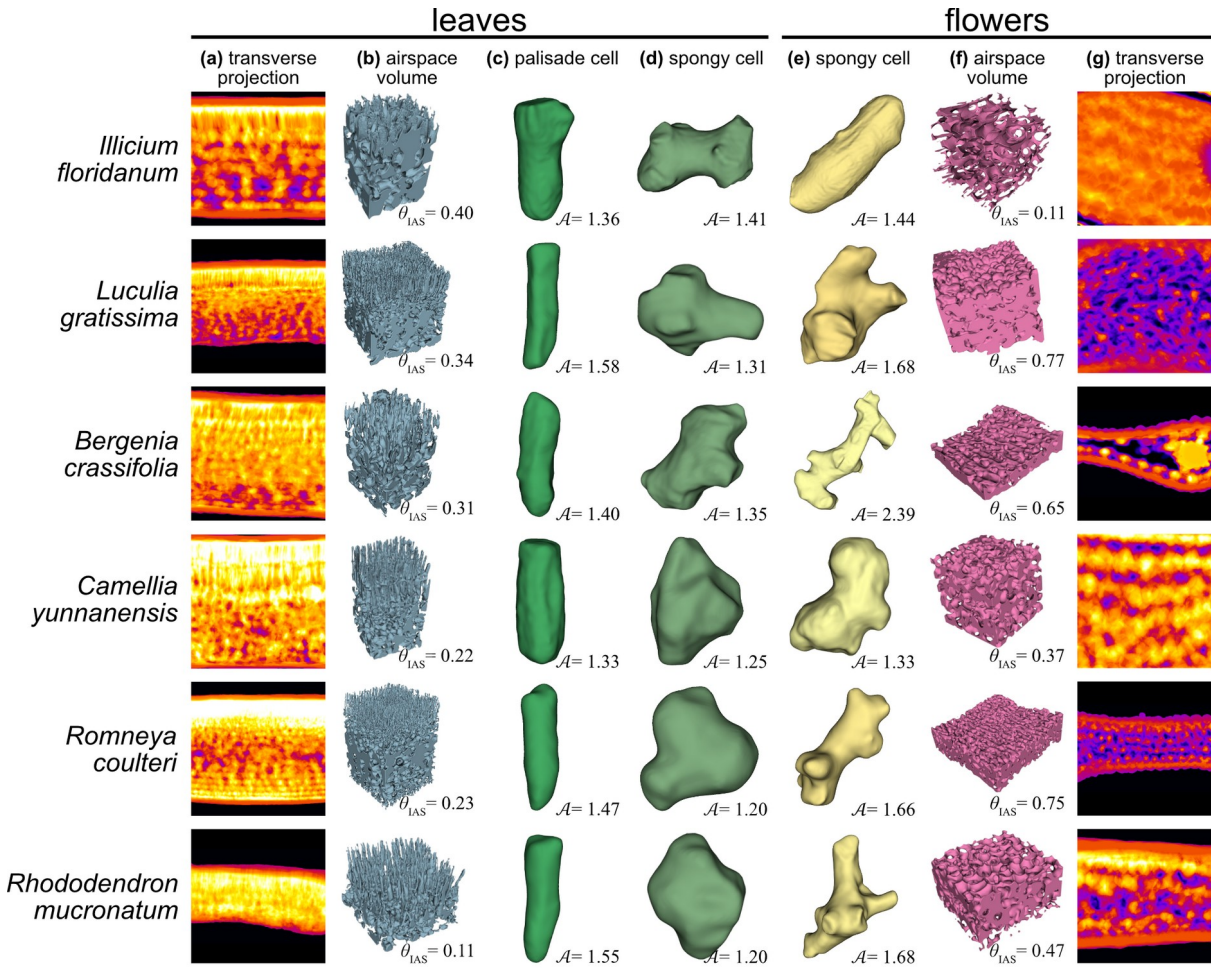

Fig. 3 Cell and tissue trait diversity among (a-d) leaves and (e-g) flowers. (a) Average cross-sectional mesophyll porosity (θ_{IAS}; $mm^3\ mm^{-3}$) for leaves, visualized by averaging across the depth of the microCT scan. Lighter colors indicate more cell material, and darker colors indicate more airspace. (b) 3D volume rendering of the intercellular airspace of leaves. Height (thickness) varies depending on the species. Numbers indicate the porosity (θ_{IAS}) of the tissue. (c) 3D volume rendering of one leaf palisade mesophyll cell from a leaf of each species. Numbers indicate the asphericity ($\mathcal{A}$) of the cell. (d) 3D volume rendering of one spongy mesophyll cell from a leaf of each species. Numbers indicate the asphericity ($\mathcal{A}$) of the cell. (e) 3D volume rendering of one spongy mesophyll cell from a flower of each species. Numbers indicate the asphericity ($\mathcal{A}$) of the cell. (f) 3D volume rendering of the intercellular airspace of flowers. Height (thickness) varies depending on the species. Numbers indicate the porosity (θ_{IAS}) of the tissue. (g) Average cross-sectional mesophyll porosity (θ_{IAS}; $mm^3\ mm^{-3}$) for flowers, visualized by averaging across the depth of the microCT scan. Lighter colors indicate more cell material, and darker colors indicate more

airspace. Note that in panels (a, g) the width and height are each 600 µm, and the tissue dimensions in panels (b,f) are 600 µm x 600 µm in the paradermal plane with variable height (thickness) depending on the sample. Cells displayed in panels (c-f) are visualized at different scales.

Structural mesophyll differences

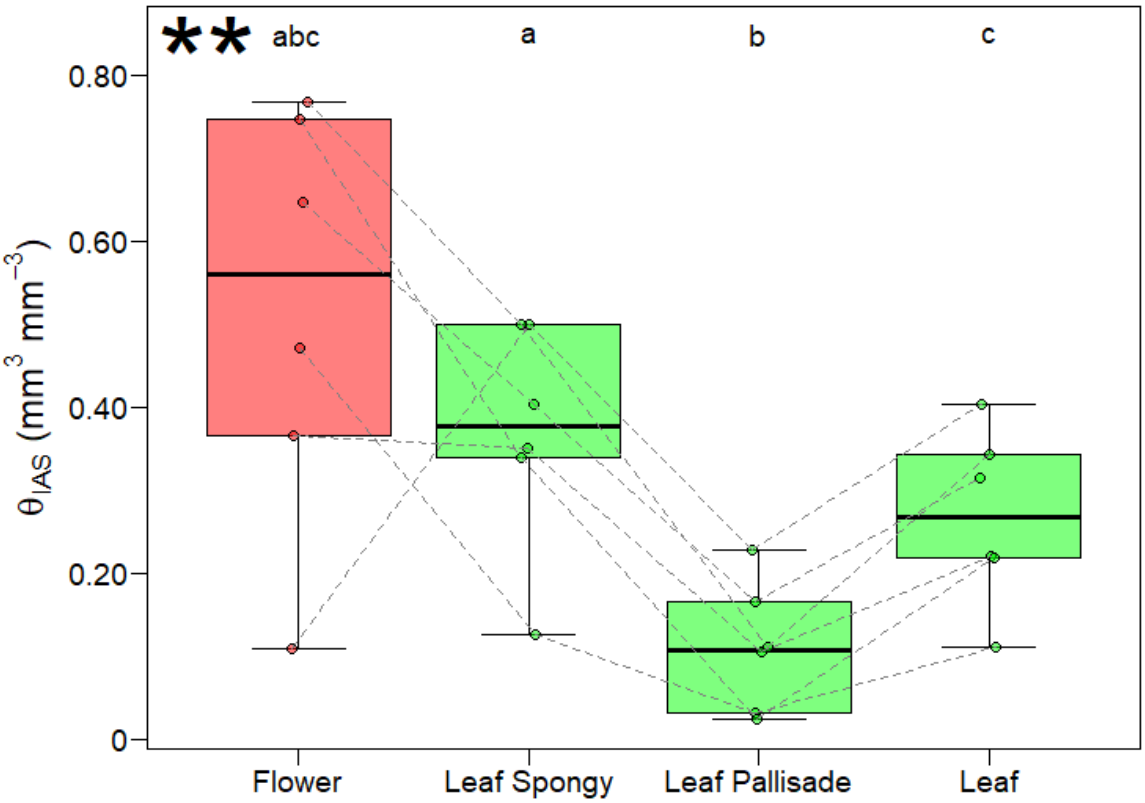

Fig. 4 Mesophyll porosity (θ_{IAS}; $mm^3\ mm^{-3}$) for the six species studied, displayed for flowers, leaf spongy mesophyll, leaf palisade mesophyll and full leaves. Letters indicate significant differences with $p < 0.05$.

Structural mesophyll differences

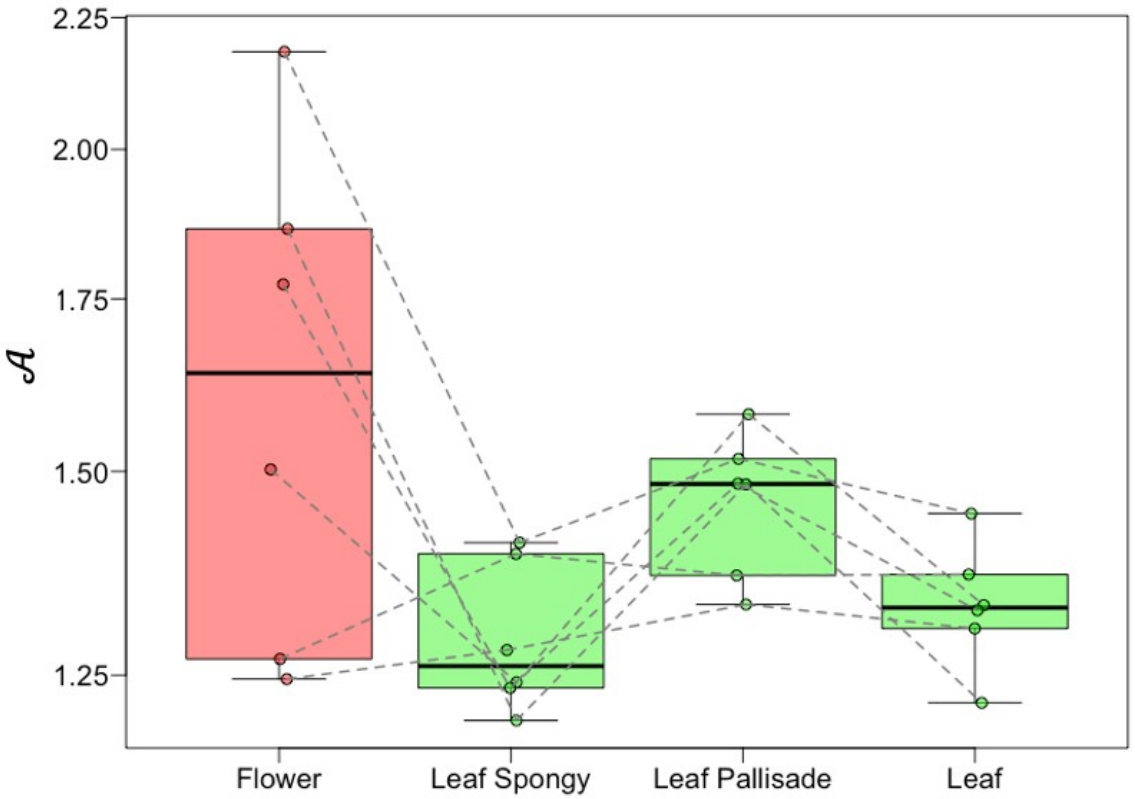

Fig. 5 Asphericity ($\mathcal{A}$) for the six species studied, displayed for flowers, leaf spongy mesophyll, leaf palisade mesophyll and full leaves.

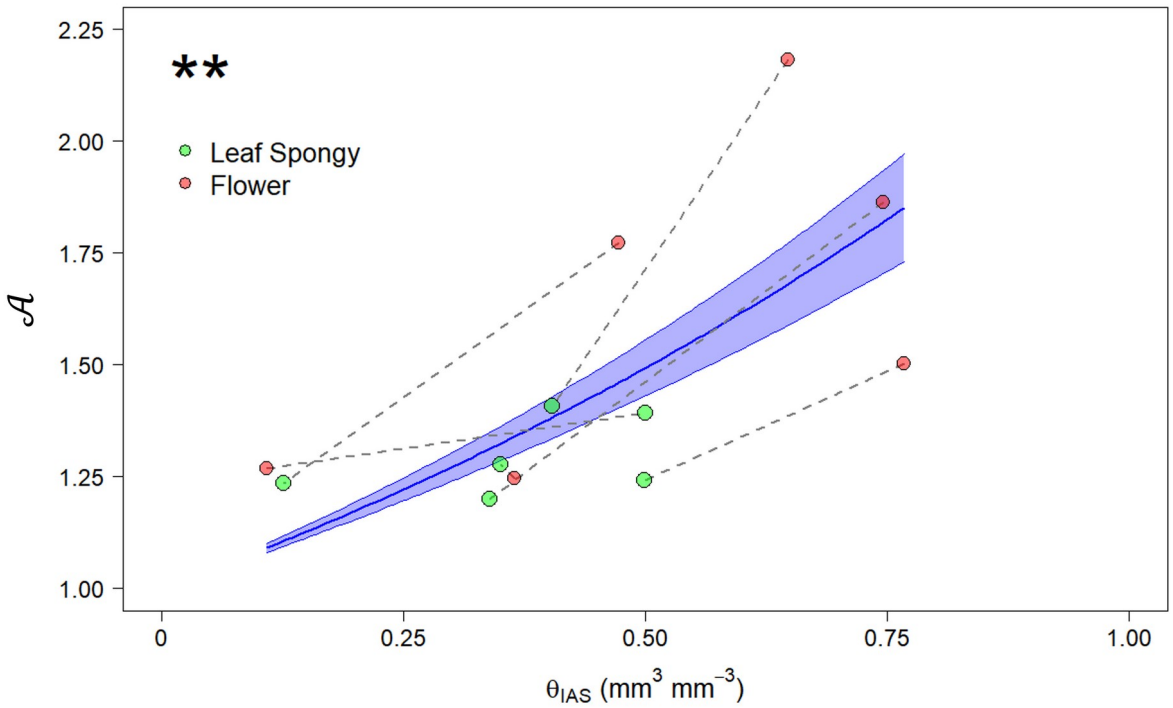

Fig. 6 Asphericity ($\mathcal{A}$) as a function of mesophyll porosity (θ_{IAS}; $mm^3\ mm^{-3}$) for the six species studied, displayed for flowers and leaf spongy mesophyll. Shaded red and green are models of the form $A = a^{\theta_{IAS}}$ for flowers and leaf spongy mesophyll, respectively. Both the model for the flowers and the leaf spongy mesophyll were significant ($p < 0.05$) with values for a of 2.35 and 1.89, respectively.

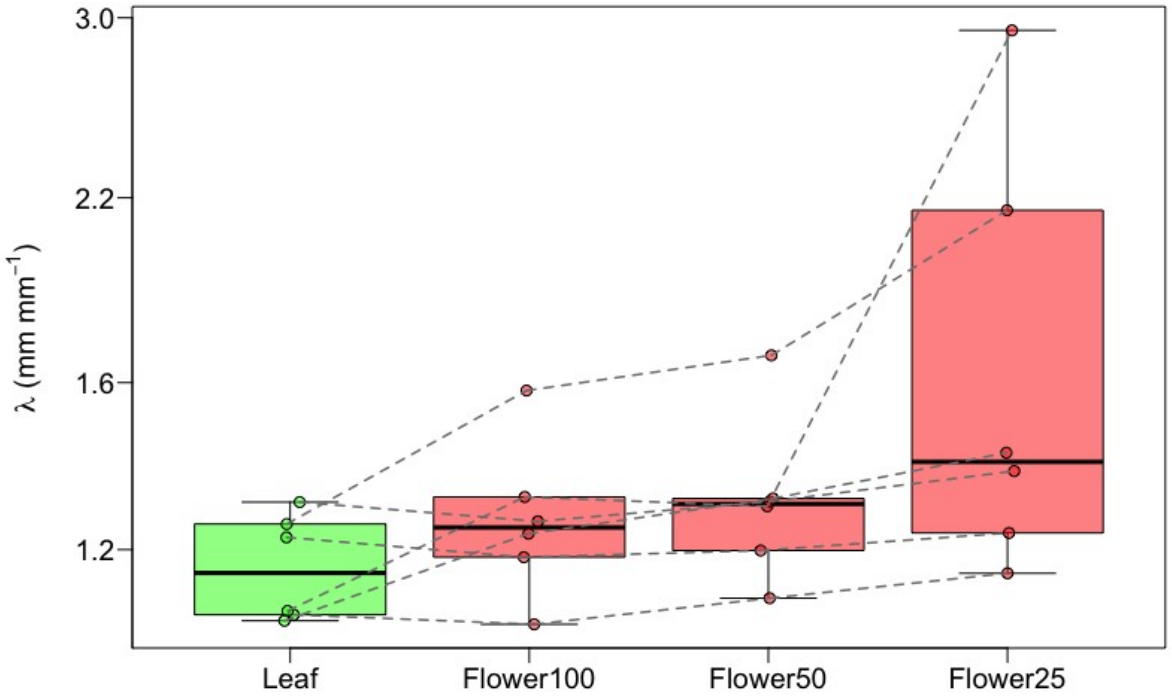

Fig. 7 Lateral path lengthening (λ; mm mm^{-1}) for the six species studied, displayed for leaves and flowers with imposed stomata similar to 100% (Flower100), 50% (Flower50) and 25% (Flower25) of the stomatal density of conspecific leaves.

Structural mesophyll differences

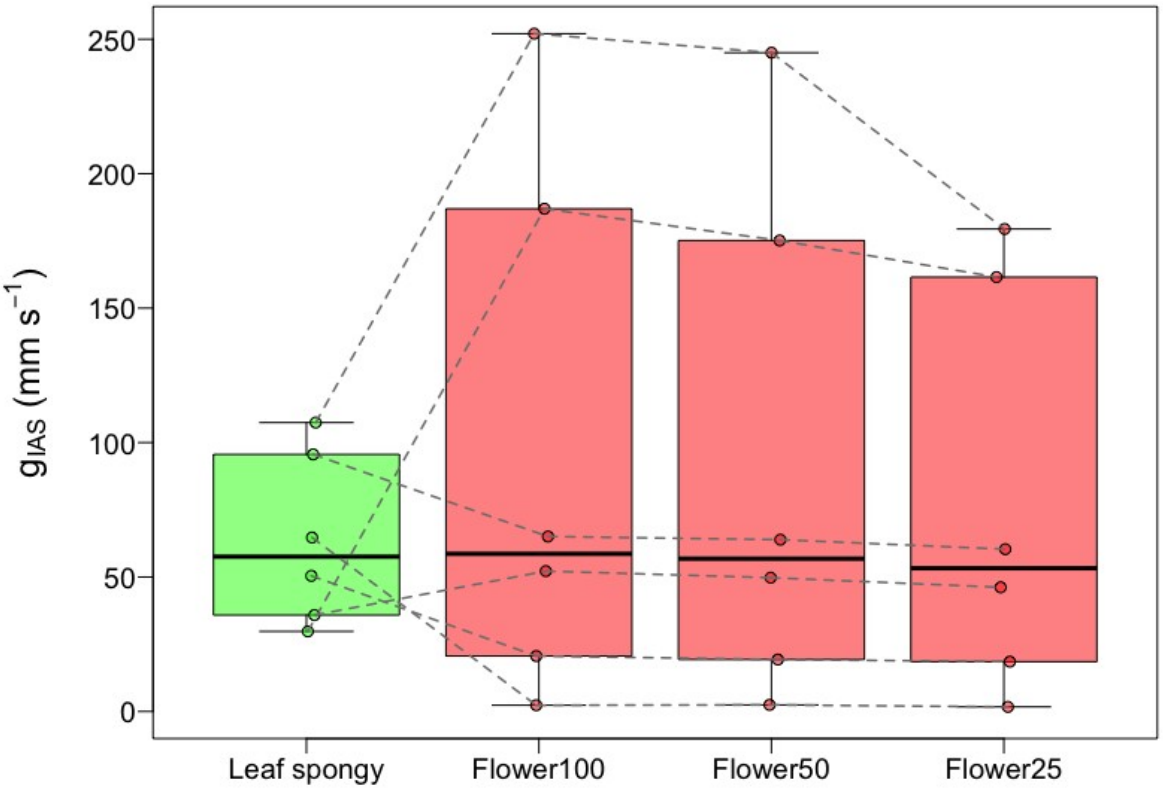

Fig. 8 Conductance of the intercellular airspace (g_{IAS}; mm s^{-1}) for the six species studied, displayed for leaf spongy mesophyll and flowers with imposed stomata similar to 100% (Flower100), 50% (Flower50) and 25% (Flower25) of the stomatal density of conspecific leaves.

Structural mesophyll differences

Supplementary data

Table S1 Phylogenetic paired t-test results for each trait

Table S2 Imposed floral and measured leaf stomatal density

Fig. S1 Workflow used for manual cell segmentation

Fig. S2 Pores observed in the epidermis of petals of *Romneya coulteri*.

Fig. S3 Vein diameter (mm) for the six species studied for flowers and leaves.

Fig. S4 The tortuosity factor (τ; mm mm^{-1}) for the six species studied, displayed for leaves and flowers with imposed stomata.

Fig. S5 The tortuosity factor (τ; mm mm^{-1}) and lateral path lengthening (λ; mm mm^{-1}) as a function of mesophyll porosity (θ_{IAS}; mm^3 mm^{-3}) for the six species studied, displayed for leaves and flowers with imposed stomata.

Fig. S6 Conductance of the intercellular airspace (g_{IAS}; mm s^{-1}) for the six species studied, displayed for leaves and flowers with imposed stomata.

Fig S7. Larger versions of the transverse projections in Figure 3.